Effect of pouring and mold temperatures on fluidity and hot tearing behavior of cast Al−Li−Cu−Mg−Sc−Zr−Ti alloy

Yi-xiao WANG[1], Guo-hua WU[1], Liang ZHANG[1], You-jie GUO[1], Xin TONG[1], Liang-bin LI[2], Xun-man XIONG[2]

1. National Engineering Research Center of Light Alloy Net Forming and State Key Laboratory of Metal Matrix Composite, School of Materials Science and Engineering, Shanghai Jiao Tong University, Shanghai 200240, China;
2. Jiangxi Ganfeng Lithium Co., Ltd., Xinyu 338004, China

Abstract: The influence of pouring temperature and mold temperature on the fluidity and hot tearing behavior of Al−2Li−2Cu−0.5Mg−0.15Sc−0.1Zr−0.1Ti alloys was investigated by experimental investigation and simulation assessment. The results showed that the length of the spiral fluidity sample increases from 302 to 756 mm as the pouring temperature increases from 680 to 740 °C, and from 293 to 736 mm as the mold temperature increases from 200 to 400 °C. The hot tearing susceptibility (HTS) firstly decreases and then increases with increasing pouring and mold temperatures, which is mainly caused by the oxide inclusion originating from the high activity of Li at excessive pouring temperature. Excessive pouring and mold temperatures easily produce oxide inclusions and holes, leading to a reduction in fluidity and an increase in HTS of the alloy. Combining the experimental and simulation results, the optimized pouring and mold temperatures are ~720 °C and ~300 °C for the cast Al−Li alloy, respectively.

Key words: pouring temperature; mold temperature; fluidity; hot tearing behavior; cast Al−Li alloy; numerical simulation

1 Introduction

Lightweight design and higher stiffness are eternal hot topics for next-generation complex structural materials in the aircraft and aerospace industries [1]. As reported, every 1% (in wt.%, unless stated) addition of Li to Al could lower the density by about 3% and increase the elastic modulus by approximately 6% [2]. Due to the significant weight reduction and modulus improvement produced by Li addition, increasing the content of Li will further meet the demands of weight-critical and stiffness-critical structural materials. Casting is not only an effective method to improve the content limit of 1.8% Li in wrought Al−Li alloys but also a low-cost way to manufacture large-size and complex structural parts [3]. However, there are currently limited investigations discussing the castability of Al−Li alloys. Castability is a complex parameter affected by the properties of the metal as well as the mold and solidification conditions. In addition, due to the high chemical activity of Li, Li-containing aluminum alloys are prone to produce oxidation inclusions and gas porosities during the smelting and casting processes, which are harmful to the mechanical properties and reliability of castings [4,5]. Therefore, it is necessary to investigate the castability of cast Al−Li alloys in order to improve quality of casting and reduce scrappage [6].

In the manufacturing of casting components, fluidity and hot tearing are two main factors affecting

the filling process and mechanical properties of casting. Fluidity, as the primary index used to evaluate alloy formability, is the major issue that must be addressed in manufacturing large-size and complex castings [7]. Metallurgical variables and mold/casting variables are the main factors that have a complex influence on fluidity. However, few investigations have focused on the fluidity of cast Al−Li alloys. Currently, the related research on the fluidity of Al−Li alloys has mainly focused on the effect of composition variations, with little attention paid to other factors such as pouring conditions, mold material and cooling rate, affecting the fluidity of Al−Li alloys [8−10].

Hot tearing, as another main index to evaluate alloy formability, is one of the most severe and irreversible casting defects for alloys [11]. Various related models and criteria have been proposed to investigate the hot tearing behavior and its occurrence mechanism [12,13]. The combination of casting and Al−Li alloys has significant practical significance for the development of casting structural parts in the direction of large-scale, lightweight and integrated structures and functions in cast Al−Li series alloys [14,15]. Unfortunately, Al−Li−Cu series alloys are prone to forming porosity and cracking during the industrial casting process. Microalloying and optimization of process parameters are effective methods to eliminate adverse effects. However, for a definite alloy composition, the related thermophysical properties, especially the melting and freezing points, have been fixed and are hard to change. The most commonly used method to prevent hot tearing is to adjust casting process parameters [16]. Furthermore, there have yet been no studies on the optimization of casting techniques. Therefore, it is of engineering significance to investigate the effect of mold/casting variables on hot tearing to further the industrial application of cast Al−Li alloys.

Recently, the Al−2Li−2Cu−0.5Mg−0.15Sc−0.1Zr−0.1Ti alloy has been a newly-developed cast Al−Li alloy that exhibits good comprehensive properties. Its density, elastic modulus, yield strength, ultimate tensile strength and elongation can reach 2.57 g/cm^3, 79 GPa, 350 MPa, 450 MPa and 4%, respectively [17,18]. Nevertheless, there still exist obstacles in large-scale popularization and application, especially in the optimization of casting properties. Fluidity and hot tearing are the main

indicators of the development of alloy melting and casting processes. Weak research in this area is one of the bottlenecks that restricts the industrial application of Al−Li alloys. In this work, the influence of the casting process on the micro-structure and properties of Al−Li alloys in permanent molds was studied. The effects of the pouring temperature and mold preheating temperature on the fluidity and hot tearing behavior of Al−2Li−2Cu−0.5Mg−0.15Sc−0.1Zr−0.1Ti alloys were systematically investigated, to provide a reference for the actual production process of Al−Li alloy casting.

2 Experimental

2.1 Alloy preparation

The Al−2Li−2Cu−0.5Mg−0.15Sc−0.1Zr−0.1Ti alloy was prepared from pure Li, Mg and Al, Al−50Cu, Al−2Sc, Al−5Zr and Al−5Ti−B master alloys in the electric resistance furnace under the protective gas of Ar. More specific preparation procedures could be available in our previous work [19]. Then, the melt was poured into a fluidity mold and a constrained rod casting (CRC) apparatus preheated to the target temperature. The related casting parameters are presented in Table 1. The actual chemical composition was determined by the inductivity couple plasma atomic emission spectroscopy (ICP-AES) analyzer, as given in Table 2.

Table 1 Parameters of casting process of Al−2Li−2Cu−0.5Mg−0.15Sc−0.1Zr−0.1Ti alloy

Pouring temperature/°C	Mold temperature/°C
680	300
700	300
720	200, 300, 400
740	300

Table 2 Chemical composition of Al−2Li−2Cu−0.5Mg−0.15Sc−0.1Zr−0.1Ti alloy (wt.%)

Li	Cu	Mg	Sc	Zr	Ti	Al
1.94	2.01	0.48	0.15	0.12	0.089	Bal.

2.2 Fluidity and hot tearing tests

A spiral fluidity testing permanent mold and a CRC mold were employed to estimate the fluidity

and hot tearing susceptibility, and schematic diagrams of the molds are shown in Fig. 1. The length of the spiral runner with a trapezoidal cavity of 10 mm in width and 5 mm in depth was 1500 mm. The dimensions of the cross-section of the mold were 300 mm × 300 mm. The actual traveled length of the melt was used to semi-quantitatively evaluate the fluidity.

The schematic diagram of the CRC mold is shown in Fig. 1(b), which is the same as that used by CAO et al [20,21]. The CRC mold consists of five constrained rods in the steel mold and a steel pouring cup. The thermocouple and load cell were applied in the longest restrained rod to capture the volumetric contraction force−temperature−time curves obtained by the data acquisition system. The other four constrained rods were used to calculate the hot tearing susceptibility (HTS) values. The HTS calculation method for gravity casting is based on an equation proposed by ARGON and BIKERMAN et al [22] and shown as follows:

$$\text{HTS} = \sum (F_{\text{length}} \cdot F_{\text{location}} \cdot F_{\text{crack}}) \qquad (1)$$

As shown in Fig. 1, the HTS value depends on the crack bar length (F_{length}), location of the crack (F_{location}) and crack severity (F_{crack}). The F_{length} values are 4 for a crack or fracture on the longest rod, 8 for a crack or fracture on the second-longest rod, and 16 and 32 for a crack or fracture on the third-longest and shortest rods, respectively. F_{location} values depend on the location of the defect, that is, 1 for a defect on the sprue end, 2 for a defect on the ball end, and 3 for a crack in the middle of the rod. The F_{crack} values are 1 for a hairline crack, 2 for a large hairline crack, 3 for a major crack, and 4 for a fracture. These details can also be found in other studies [24]. The HTS of each alloy was evaluated three times, and the average value was used for discussion.

2.3 Numerical simulation modeling

In this work, the software ProCAST was used to simulate the casting and solidification processes based on the finite element. The hot tearing indicator (HTI) module proposed by GURSON et al [23] was employed to evaluate the HTS of the studied alloy. The related equation is as follows:

$$\text{HTI} = e_{\text{ht}} = \overline{\varepsilon}_{\text{ht}}^{\text{p}} = \int_{t_{\text{c}}}^{t_{\text{s}}} \sqrt{\frac{2}{3} \dot{\varepsilon}^{\text{p}} / \dot{\varepsilon}^{\text{p}}} \, \text{d}\tau, \quad t_{\text{c}} \le t \le t_{\text{s}} \qquad (2)$$

where $\overline{\varepsilon}_{\text{ht}}^{\text{p}}$ is the critical accumulated effective plastic strain for the initiation of hot tearing, $\dot{\varepsilon}^{\text{p}}$ is the effective plastic strain rate, t_{c} is the time when dendrite coherence starts, t_{s} is the solidus temperature, and τ is the dyadic parameter. In the numerical simulations of fluidity and hot tearing behavior, the heat transfer coefficient of the ingot−mold interface and the ambient temperature were 750 W/(m²·K) and 25 °C, respectively. The pouring and mold temperatures were set to be the target temperatures, and the related parameters are illustrated in Table 1. To obtain accuracy results and reduce calculation amount, the element size of the spiral fluidity sample and constrained rod was set to 1 mm, the element sizes of the mold and pouring cup were considered as 2 and 2.5 mm, respectively. More specific simulation parameters and boundary conditions could be found in previous work [24,25].

2.4 Microstructural characterization

The specimens for the hot tearing tests (near the hot tears in the sprue) were polished and etched by standard metallographic polishing methods and Keller's reagent, respectively. The specimens were etched by Keller's reagent for 15 s prior to the characterization. The phase composition and thermal properties were calculated with Pandat software 2021 and JMatPro 7.0 software, respectively. Optical microscopy (Axion Observer A1, OM) and
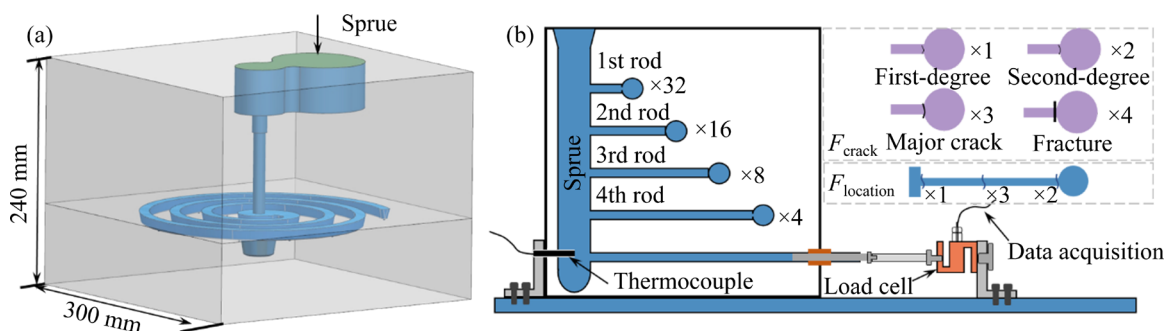

Fig. 1 Schematic diagrams of fluidity apparatus (a) and CRC mold (b)

scanning electron microscopy (Phenom XL, SEM) were used to observe the microstructure of the studied alloys. Energy dispersive X-ray spectroscopy (EDS) was adopted to analyze the distribution of alloying elements. To ensure reliability, more than 20 images were used. The grain sizes, secondary phase fractions and particles were analyzed by Image-Pro Plus software. A digital camera was employed to take photos of the hot tearing cracks. To analyze the distribution of Li and O elements, an SEM (GAIA3) apparatus equipped with a time-of-flight secondary ion mass spectrometer (TOF-SIMS) was used to determine the microstructure. Rod-shaped samples of 9 mm in diameter and 15 mm in length were used for XCT analysis. According to the difference in image contrast caused by different densities of samples and crack, the region with low gray values was extracted as hot tearing crack. The X-ray microscopy (XRM ZRISS Xradia 520 Versa) system operated at an acceleration voltage of 100 kV and a power of 9.0 W with a pixel size of 10.054 μm was adopted for the 3D morphology of the hot tearing crack. During data processing using Dragonfly commercial software, the sample size of XCT scan was 9 mm × 9 mm and defects below 9

voxels were eliminated to reduce noise interference. To obtain accuracy results and avoid image distortion, over 1000 slices and threshold processing method were applied during data processing.

3 Results

3.1 Effect of pouring and mold temperatures on fluidity

Figure 2 shows the simulation and experiment results of fluidity samples at different pouring temperatures. Based on the simulation results, the fluidity lengths for the studied alloys at 680, 700, 720 and 740 °C were 335, 556, 621 and 767 mm, respectively. According to the experiment results, the length of the spiral fluidity sample of the Al−2Li−2Cu−0.5Mg−0.15Sc−0.1Zr−0.1Ti alloy was 302 mm at a pouring temperature of 680 °C. As the pouring temperature increased from 680 to 700 °C, the length of the spiral fluidity sample was increased by 66%. As the pouring temperature further increased, the fluidity lengths at 720 and 740 °C were 603 and 756 mm, respectively. The simulated results are basically consistent with the experimental results. When the pouring temperature increased
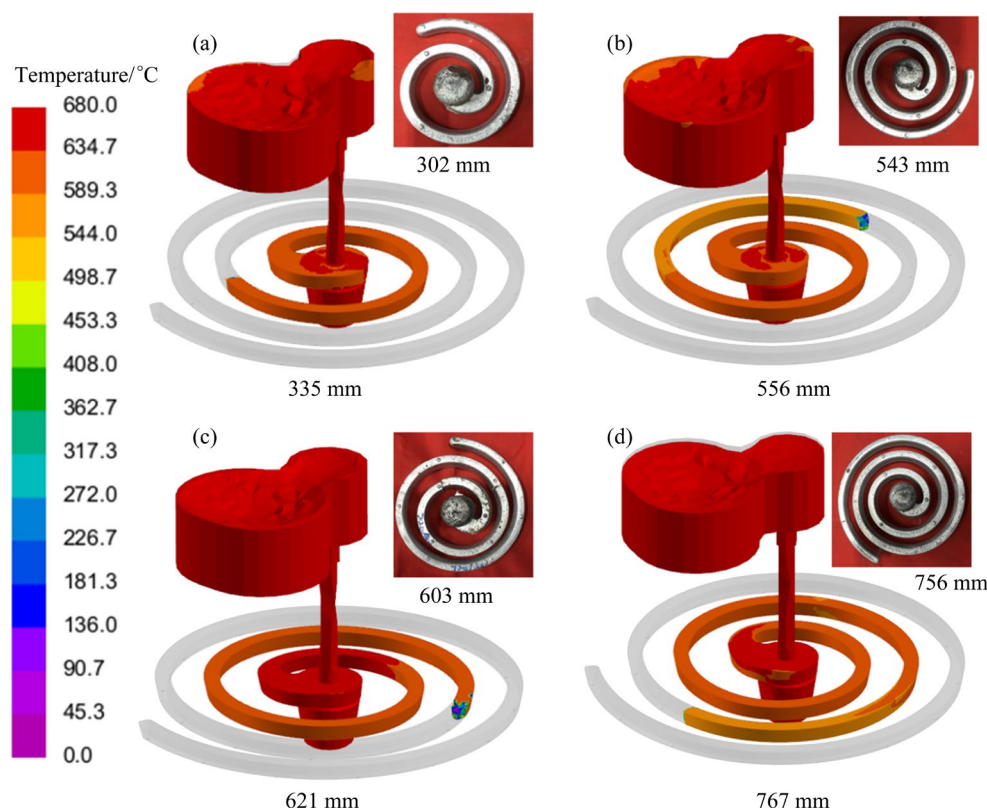

Fig. 2 Simulation and experiment results of fluidity at different pouring temperatures: (a) 680 °C; (b) 700 °C; (c) 720 °C; (d) 740 °C

from 680 to 740 °C, the increase amplitude in fluidity length gradually decreased and then increased. It can be concluded that the increase in pouring temperature could significantly improve the fluidity of the alloy in the range of 700−740 °C, while there is a limit.

To investigate the effect of different mold temperatures on the fluidity of the cast Al−2Li−2Cu−0.5Mg−0.15Sc−0.1Zr−0.1Ti alloy, the simulated and experimental data of fluidity samples are shown in Fig. 3. According to the simulation results, the lengths of the spiral fluidity samples at mole temperatures of 200, 300 and 400 °C were 307, 621 and 758 mm, respectively. With increasing mold temperature, an increase in the fluidity length was in good agreement with experiment results of 293, 603 and 736 mm, respectively. The simulation and experiment results agree well with each other, so the accuracy of the numerical results is validated. In addition, the results of computer simulation and experiment both show that an increasing trend could be found in fluidity with increasing mold temperature.

Based on the aforementioned fluidity comparison, increasing the pouring temperature demonstrates a distinct advantage over elevating the mold temperature for an equivalent temperature increment. Thermal field analysis indicates that the flow front in the spiral fluidity test ceases prematurely, while significant residual liquid persists within the spiral cavity. These observations suggest that when the advancing metal reaches a critical viscosity threshold, localized viscosity buildup occurs, ultimately leading to flow termination.

3.2 Effect of pouring and mold temperatures on hot tearing susceptibility

Table 3 shows all cracks and fractures of the studied alloys at different pouring temperatures. The studied alloy suffered a second-degree minor crack at the sprue of the second rod and a fracture at
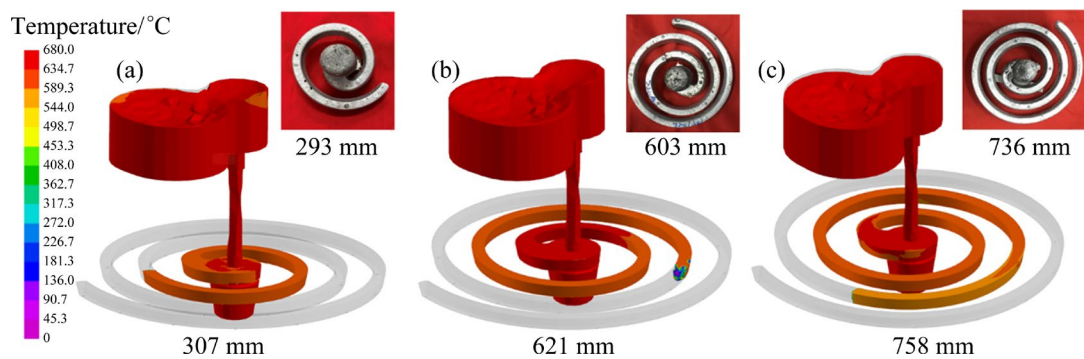

Fig. 3 Simulation and experiment results of fluidity at different mold temperatures: (a) 200 °C; (b) 300 °C; (c) 400 °C

Table 3 Crack fractures of hot tearing for studied alloy at different pouring temperatures

Rod No.	680 °C	700 °C	720 °C	740 °C
1st	No crack	No crack	No crack	No crack
2nd	Second-degree minor crack	No crack	No crack	No crack
3rd	Fracture	Major crack	No crack	No crack
4th	Fracture	Fracture	First-degree crack	Fracture

the sprue of the third and fourth rods when the pouring temperature was 680 °C. As the pouring temperature increased to 700 °C, a major crack at the sprue of the third rod and a fracture at the sprue of the fourth rod could be observed. As the pouring temperature increased to 720 °C, the cracks at the sprue of the fourth rod suffered a first-degree crack. However, a fracture morphology at the sprue of the fourth rod was obtained in the studied alloy when the pouring temperature was 740 °C, indicating a poor resistance to hot tearing. According to Eq. (1), the HTS values of the studied alloy at 680, 700, 720 and 740 °C were 80, 40, 4 and 16, respectively. The tendency of hot cracking first decreased and then increased.

To quantify the stress value during solidification, volumetric contraction force−temperature−time curves of the studied alloys at different pouring temperatures are shown in Fig. 4. The load represents the tensile force developing during casting due to solidification shrinkage and thermal contraction. Drop-in (DI) contraction forces indicate the occurrence of hot tearing due to stress relaxation [26,27]. The experiment results indicate that the values of the DI force for the studied alloy with pouring temperatures of 680, 700, 720 and 740 °C were calculated to be 22.3, 17.5, 14.3 and

23.47 N, respectively. It is striking that the pouring temperature of 740 °C brought about a large gap in the DI force, which means that the studied alloy has a high hot crack trend. Therefore, a proper decrease in pouring temperature contributes to reducing the tendency of hot crack for the studied alloy.

Table 4 shows all cracks and fractures of the studied alloys at different mold temperatures. The studied alloy suffered a second-degree minor crack at the sprue of the second rod, a major crack at the sprue of the third rod and a fracture at the sprue of the fourth rod when the mold temperature was 200 °C. When the mold temperature increased to 300 °C, a first-degree crack at the sprue of the fourth rod could be observed. As the mold temperature increased to 400 °C, there were no cracks in the CRC mold, indicating better casting properties. According to Eq. (1), the HTS values at mold temperatures of 200, 300 and 400 °C were 96, 4 and 0, respectively. As the mold temperature increased from 200 to 400 °C, the tendency of hot tearing gradually decreased. Comparing the pouring temperature and mold temperature, too high pouring temperature is unfavorable to the casting properties of the studied alloy, while an increase in the mold temperature is conducive to improving the fluidity and inhibiting the occurrence of hot tearing.
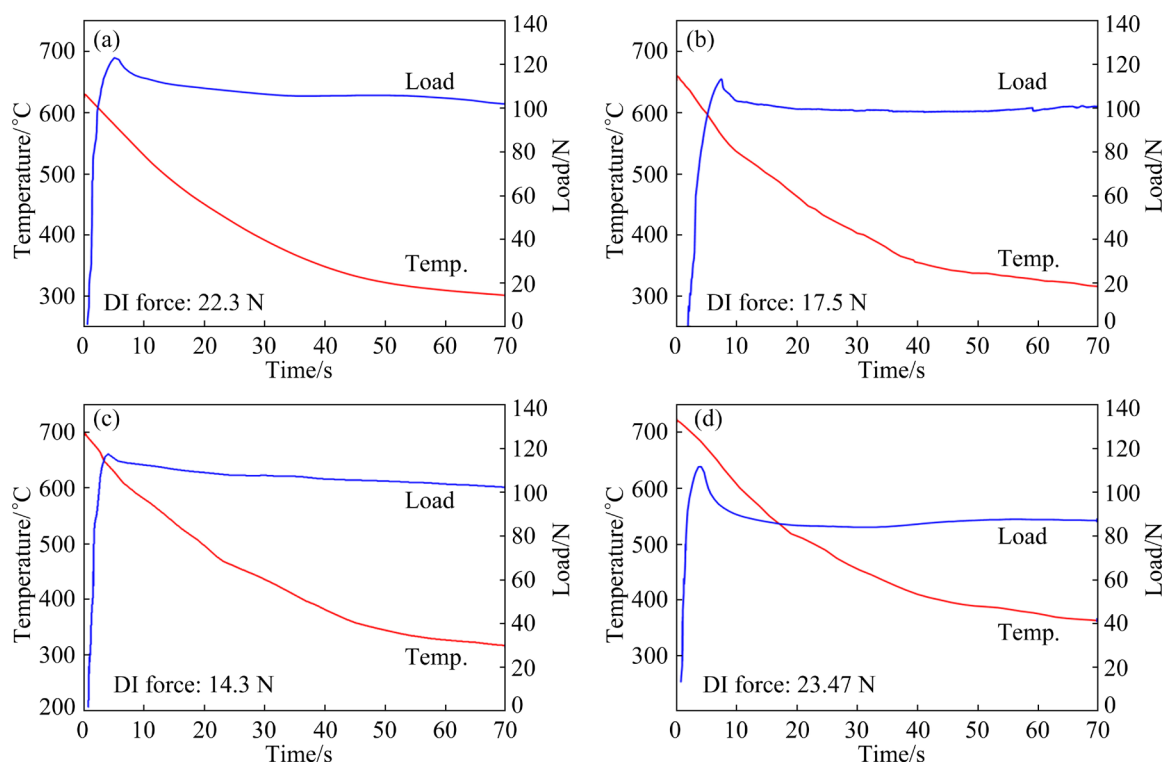

Fig. 4 Volumetric contraction force (load)−temperature−time curves of studied alloy at different pouring temperatures: (a) 680 °C; (b) 700 °C; (c) 720 °C; (d) 740 °C

Similarly, the volumetric contraction force−temperature−time curves of the studied alloy at different mold temperatures are shown in Fig. 5. The values of DI force for the studied alloy at mold temperatures of 200, 300 and 400 °C were calculated to be 16.1, 14.3 and 11.6 N, respectively. The DI force gradually decreased as the mold temperature increased. It could be recommended that the filling velocity of the molten alloy is faster and the hot tearing resistance is higher with the increase of mold temperature.

The occurrence of oxides increases the hot tearing susceptibility of the alloys, leading to macroscopic shrinkage cavities and porosity. The Niyama criterion was used to evaluate the shrinkage cavity and porosity, which can be expressed as follows [28]:
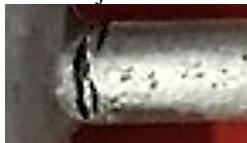
$$G/\sqrt{R} = \sqrt{\frac{\eta \cdot f_{L} \cdot \beta \cdot \Delta T}{K \cdot (\Delta P - m \cdot \Delta T \cdot g/A)}} \quad (3)$$

where G is the temperature gradient, R is the cooling rate during solidification, η is the liquid phase viscosity coefficient, f_{L} is the liquid fraction, β is the shrinkage rate of solidification, K is the interdendritic permeability, ΔP is the pressure drop, m is the slope coefficient between temperature gradient and pressure difference, ΔT is the interval of crystallization temperature, g is the gravitational acceleration, and A is the length of the spiral fluidity sample. According to Eq. (3), the Niyama criterion is derived by combining the growth mechanism of dendrites in the mush region with the theory of seepage feeding. Figure 6 presents the shrinkage porosity calculated by the Niyama criterion and hot tearing indicator. The positions of shrinkage porosity are consistent with the maximum value of hot tearing cracking, which means that larger stress values may result in shrinkage porosity.

To better understand the formation of hot tearing cracks, XRM analysis was adopted to construct the 3D morphology of cracks to reveal the

Table 4 Cracks and fractures of hot tearing for studied alloy at different mold temperatures

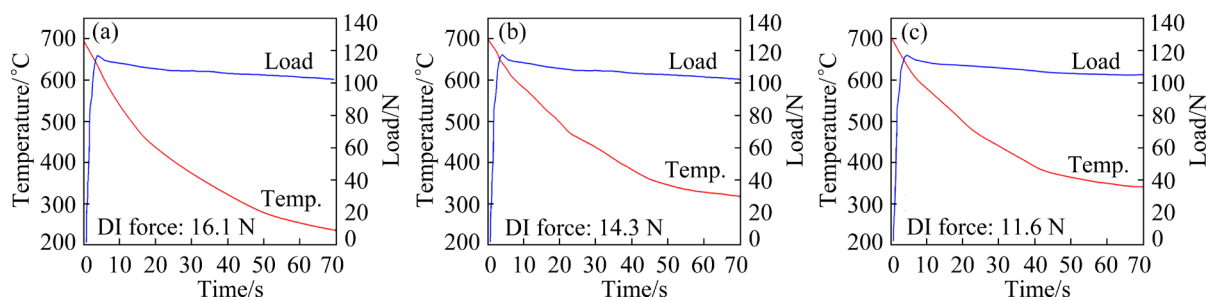| Rod No.	200 °C	300 °C	400 °C
1st	No crack	No crack	No crack
2nd	Second-degree minor crack	No crack	No crack
3rd	Major crack	No crack	No crack
4th	Fracture	First-degree crack	No crack

Fig. 5 Volumetric contraction force (load)−temperature−time curves of studied alloy at different mold temperatures: (a) 200 °C; (b) 300 °C; (c) 400 °C

initiation and propagation of cracks. As displayed in Fig. 7, the representative viewing region was cut from the studied alloy under the conditions of a pouring temperature of 720 °C and a mold temperature of 300 °C. The mid-plane, 3D morphological reconstruction and crack extraction are shown in Figs. 7(a−c), respectively. Because solidification shrinkage and unequal thermal contraction are inhibited during solidification, the applied strain is preferentially concentrated at hot-spot sites on the alloy's surface. When the produced strain exceeds the limit that the solid network can withstand, hot fissures form. The major cracks eventually expand to the sample's interior, accompanied by the development of a large number of secondary cracks. As seen in Fig. 7(c), the hot crack feature can be more clearly seen, indicating that the sample has grown to contain numerous massive interconnected cracks with a 3D reticular structure.

Figure 8 presents the SEM images of the studied alloy at different pouring temperatures and the representative EDS data. The grain size increased from (41.6±15.3) to (115.8±21.3) μm, and the area fraction of the secondary phase decreased from 3.2% to 1.7% with increasing pouring temperature from 680 to 720 °C. When the pouring temperature increased to 740 °C, some oxide inclusions and cracks could be found in the interior of the grains. According to our previous work [24], Li-rich oxide inclusions consisted of Li_2O, Li_2CO_3 and $LiAlO_2$. Based on the XRD and calculation results from our previous investigation [17], the primary particles mainly consisted of Sc and Zr, and the secondary phases were mainly composed of Cu and Mg along the grain boundaries (Fig. 8(e)). It could be recommended that the microstructure and secondary phase could be improved by properly increasing the pouring temperature, but some oxide inclusions and cracks were distributed in the interior of the grains when the pouring temperature was 740 °C. Therefore, the initial pouring temperature of the studied alloy does not exceed 740 °C during the casting process.

The SEM images and EDS data of the studied alloy at different mold temperatures are shown in Fig. 9. The grain size increased from (43.4±10.2) to
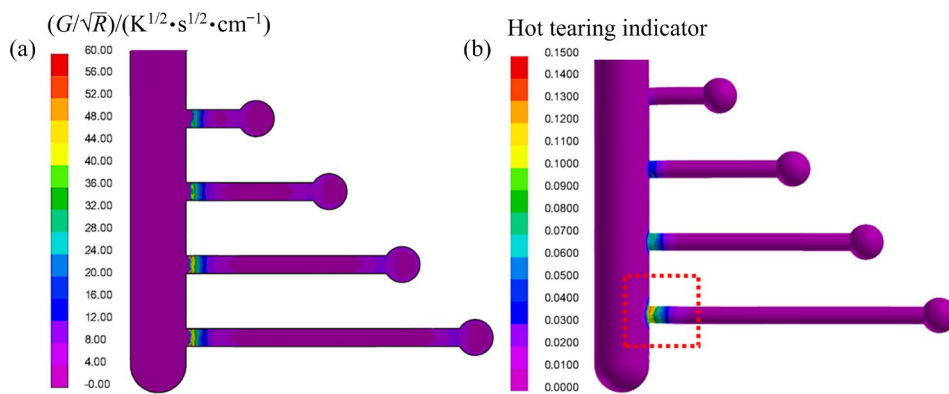

Fig. 6 Simulation results of Niyama criterion (a) and hot tearing indicator (b)
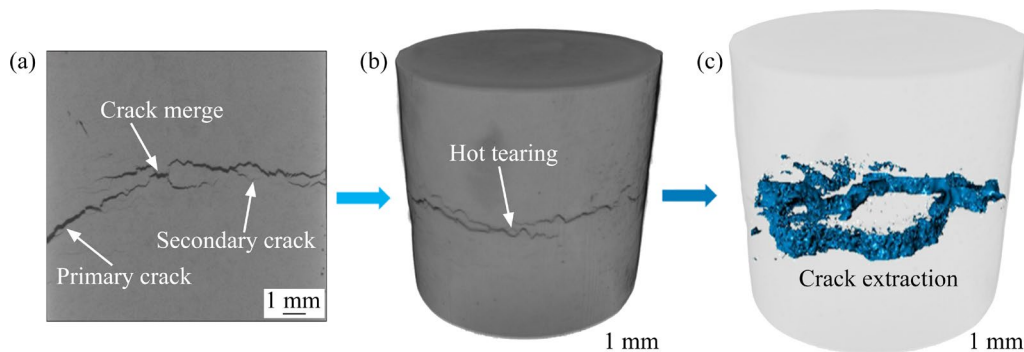

Fig. 7 Crack morphologies of hot tearing in constrained rod: (a) Typical XRM image; (b) 3D morphological reconstruction; (c) Hot cracks extracted from (b)
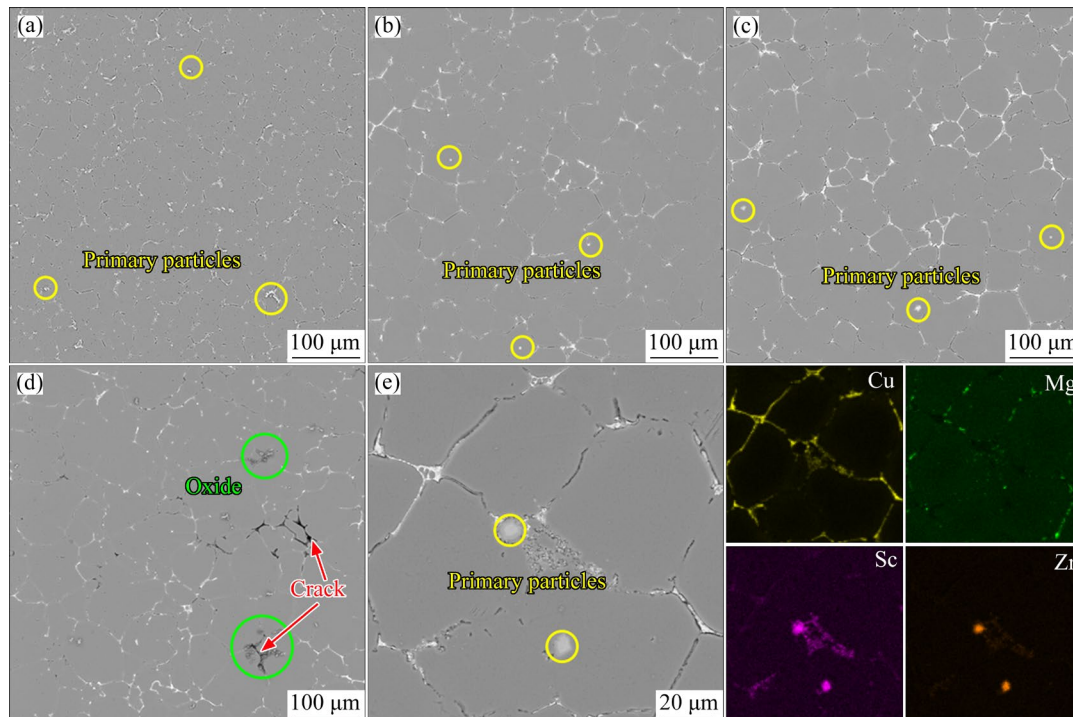
Fig. 8 SEM images of studied alloy at different pouring temperatures: (a) 680 °C; (b) 700 °C; (c) 720 °C; (d) 740 °C; (e) Primary particles and corresponding element scanning maps at pouring temperature of 720 °C
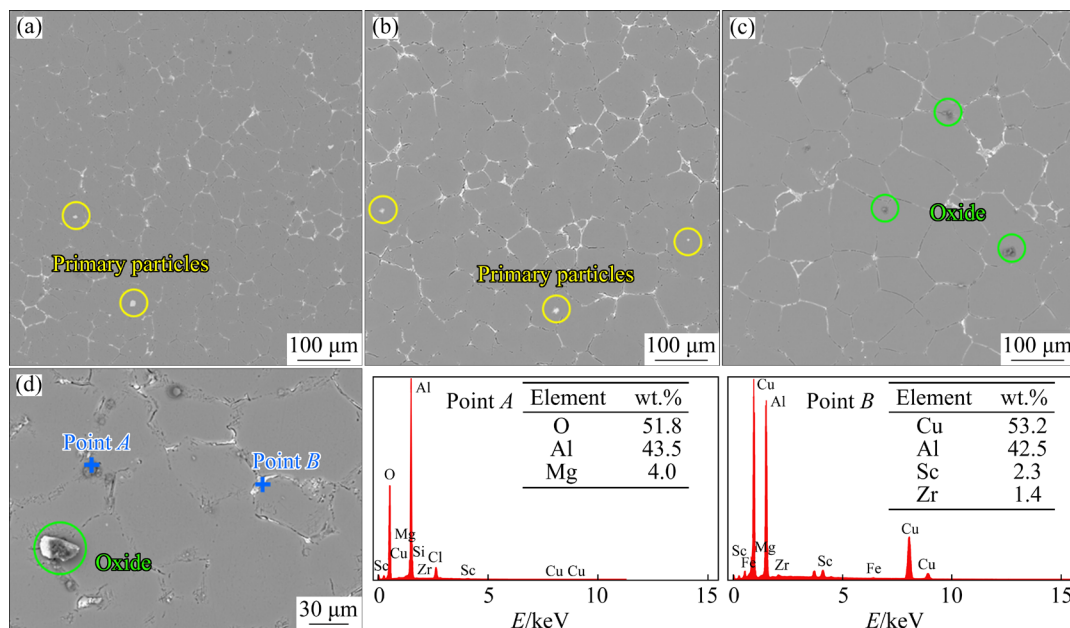

Fig. 9 SEM images and EDS data of studied alloy at different mold temperatures: (a) 200 °C; (b) 300 °C; (c) 400 °C; (d) Enlarged image of (c) and corresponding EDS analysis results

(108.2±9.67) μm and the area fraction decreased from the 2.3% to 0.9% with increasing mold temperature from 200 to 400 °C. When the mold temperature increased to 400 °C, oxide inclusions could be found in the interior of the grains, and the composition of which contained lots of O element.

Although the increase in mold temperature could alleviate the hot tearing, oxide inclusions may act as initiation sites for hot tearing cracks, resulting in the initiation and propagation of cracks. Therefore, the mold temperature for the investigated alloy must remain below 400 °C during casting.

Figure 10 displays typical SEM images of the hot tearing fracture morphology of the studied alloy at pouring temperatures of 720 and 740 °C. The hot tearing surface is bumpy, and Cu-rich phases and holes could be found in the fracture. When the pouring temperature is 720 °C, there are apparent holes on the fracture surface, which is attributed to the insufficient filling caused by the scarcity of the liquid phase at the end of solidification. As the pouring temperature increased to 740 °C, the oxide inclusions were unevenly distributed in the vicinity of the grain boundaries. Crack morphology and EDS analysis results indicate that the oxide inclusions are enriched in Cu and Li, although Li cannot be detected due to its low atomic number.

4 Discussion

4.1 Effect of pouring conditions on fluidity

Based on the above results, fluidity is generally proportional to the pouring temperature and mold temperature, which is closely related to constitutional undercooling. According to the following equation [7,29]:

$$L_f = \frac{\rho_m dv}{2h(T - T_0)}(\Delta H + C_p \Delta T)(1 + \frac{k}{2}) \qquad (4)$$

where L_f is the length of flow, ρ_m is the density of the permanent mold, d is the thickness of the casting, v is the metal flow velocity, h is the heat transfer coefficient, T is the temperature of the metal, T_0 is the temperature of the permanent mold, ΔH is the latent heat of the studied alloys, C_p is the specific heat capacity of the liquid alloy, ΔT is the undercooling, and k is the thermal conductivity. Equation (4) shows that increasing superheat could significantly improve the fluidity. In addition, the constitutional undercooling decreased with increasing pouring temperature. Once the amount of solid in the melt reached a critical fraction or the dendrites overlapped with each other (dendrite coherency), the dendrites interlocked and formed a network, making the liquid metal stop flowing [13,30]. The dendrite coherency temperature was a key factor that affected the fluidity.

Notably, fluidity is a complex parameter affected by the alloy composition and solidification conditions, which can vary the viscosity, surface tension, freezing range and solidification mode. To analyze the thermophysical parameters of the studied alloys at different pouring temperatures, JMatPro 7.0 software was used to calculate the linear expansion coefficient, thermal conductivity and liquid viscosity, as shown in Fig. 11. Figure 11(a) shows the relationship between pouring temperature and cooling rate, where the cooling rate is inversely
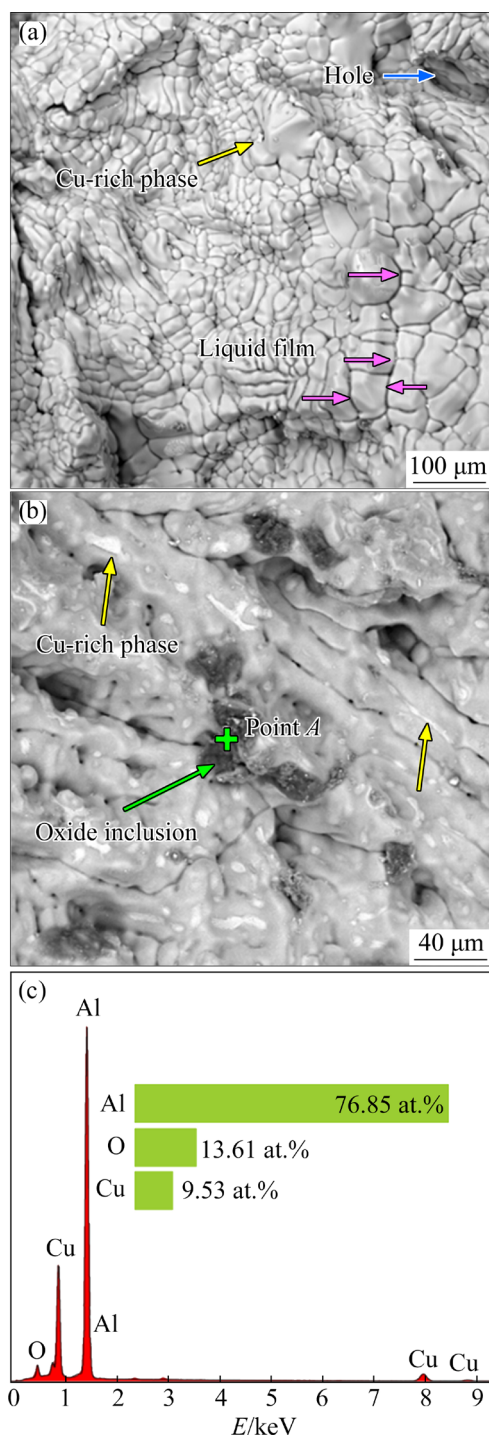

Fig. 10 Crack morphology of studied alloy at pouring temperatures of 720 °C (a) and 740 °C (b), and EDS data of Point A (c)
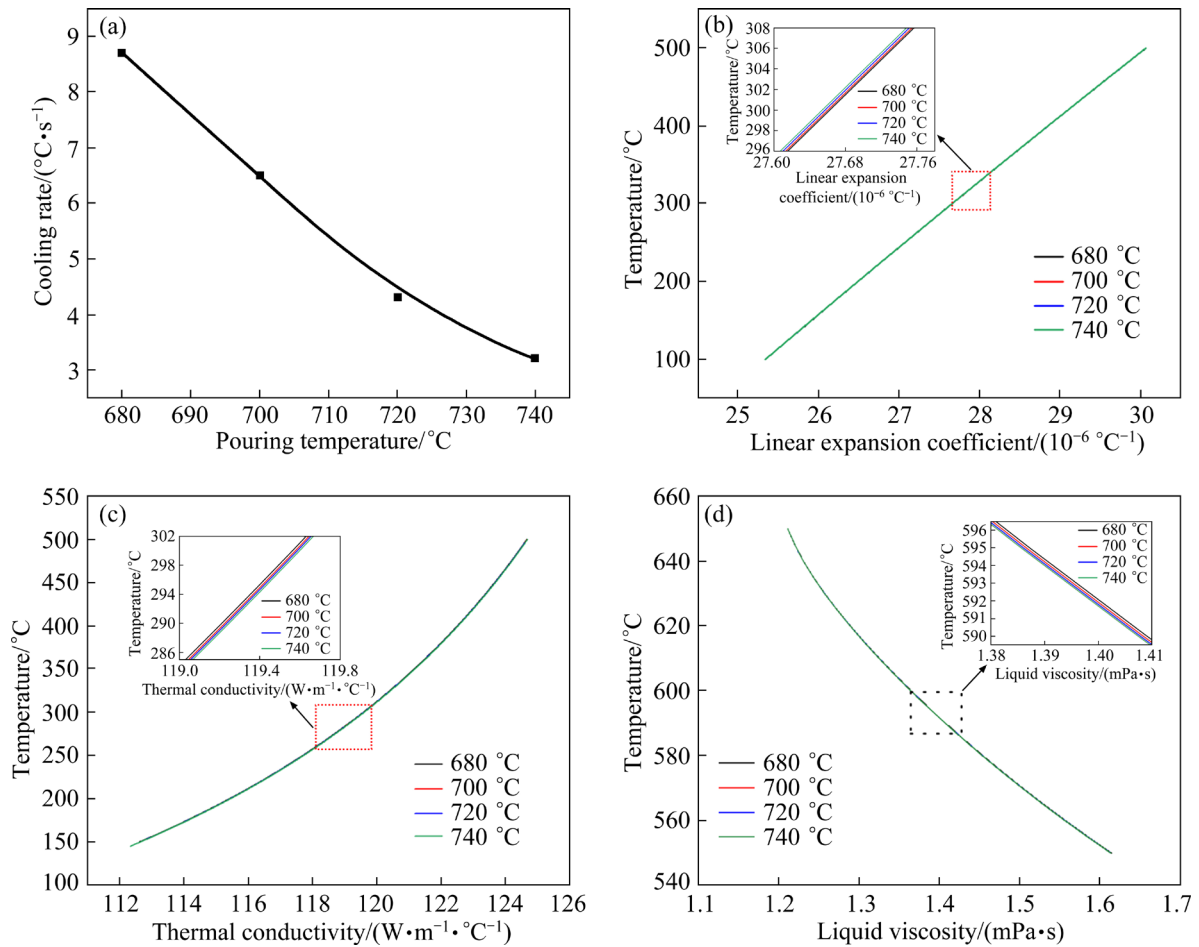
Fig. 11 Effect of pouring temperature on physical parameters: (a) Relationship between cooling rate and pouring temperature; (b) Linear expansion coefficient; (c) Thermal conductivity; (d) Liquid viscosity

proportional to the pouring temperature. The constitutive undercooling decreased with increasing pouring temperature, which is related to the linear expansion coefficient, thermal conductivity and liquid viscosity, as displayed in Figs. 11(b−d), respectively. The linear expansion coefficient and thermal conductivity increase with increasing pouring temperature. In addition, the liquid viscosity of the studied alloy decreases with increasing pouring temperature. The reduced liquid viscosity contributes to improving the fluidity of the melt at the final stage of solidification.

4.2 Effect of pouring conditions on hot tearing

In Al−Li alloys, some oxide inclusions could be found in the microstructure of the alloy due to the high activity of Li. However, the presence of oxide and oxide films easily results in the initiation and growth of cracks [31]. Unfortunately, a limited investigation has been performed to explore the

effect of Li on hot tearing. To avoid oxidation due to long placement, the specimens were characterized immediately after casting. Figure 12 presents the location and content of (Li,O)-containing phases observed by TOF-SIMS. Li and O are not evenly distributed on the grain surface. However, none of the oxide inclusions is generated by Li. Therefore, there should be some possible reaction pathway resulting in the formation of oxides. According to previous work [32], the H content in Al−Li alloys is approximately five times higher than that of commercial aluminum alloys. A strong binding energy between H and O further increases the oxide inclusion.

During the solidification of aluminum alloy, the presence of oxides and oxide films is not conducive to the mass production of casting, which act as initiation sites for hot tearing cracks and easily cause casting rejection [33]. As shown in Figs. 4 and 5, the DI contraction forces decreased

with increasing pouring and mold temperatures, which could inhibit the occurrence of hot tearing. However, as presented in Figs. 8, 9 and 12, excessively high temperature brought about the presence of the Li-containing oxide, leading to the fracture (Table 3). When the pouring and mold temperatures are lower than the critical levels, the fluidity and hot tearing behavior could be improved simultaneously. Once the pouring and mold temperatures rise, oxides and oxide films play an important role in hot tearing. Therefore, the pouring and mold temperatures should be controlled below 740 and 400 °C, respectively.

In fact, the variation of pouring condition changes the interval of constitution undercooling [34,35]. The higher the pouring temperature is, the slower the cooling rate is, and the smaller the undercooling is. During the solidification process, the increased pouring temperature and mold temperature lowered the cooling rate and the interval of the solid−liquid interface (marked by dashed blue lines in Fig. 13(a)). Then, the length of the mush broadens with increasing the pouring temperature, which can make more melt flow into the gap of the dendritic crystal. During solidification and contraction, the shrinkage stress gradually increased and further promoted the formation of minor cracks when the shrinkage stress reached a critical value (Fig. 13(a)). The occurrence of oxide inclusions containing Li and O provides sites for the initiation and expression of cracks. On the one hand, the melt contains a large number of oxide inclusions that hinder liquid feeding during the solidification of alloys. On the other hand, the occurrence of solidification shrinkage and thermal contraction due to uneven thermal gradients can impose stresses and strains on the semi-solid network [36]. In addition, micro-oxide inclusion provides initiation sites for the dilaceration of the thin liquid film (Fig. 13(b)). With the continuous accumulation of shrinkage stress, the combined effect promotes further expansion of microcracks [12].
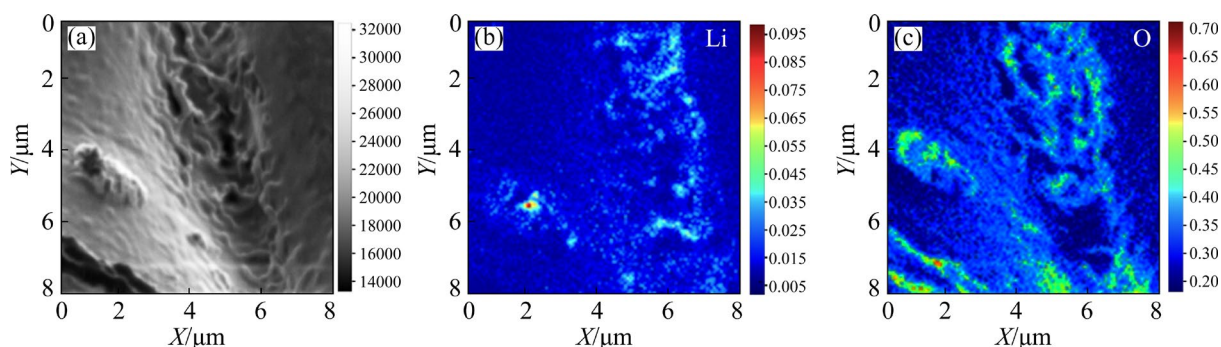

Fig. 12 TOF-SIMS images of interdendritic area for studied alloy: (a) Microstructure of sample; (b) Li element; (c) O element
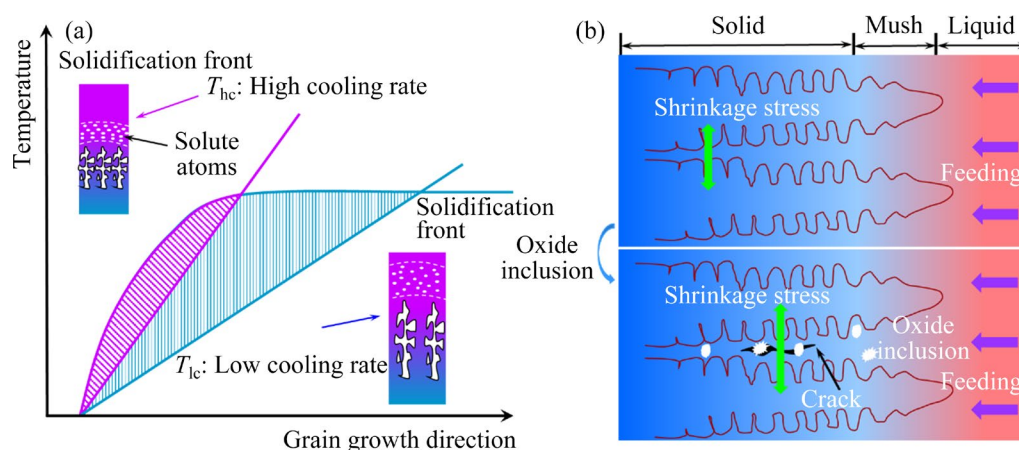

Fig. 13 Schematic illustration showing effect of cooling rate on undercooling zone, temperature gradient and solute distribution in liquid−solid interface front (a) and effect of oxide inclusions on hot tearing (b)

5 Conclusions

(1) As the pouring temperature increased from 680 to 740 °C, the length of spiral fluidity sample of the Al−Li−Cu−Mg−Sc−Zr−Ti alloy increased from 302 to 756 mm, the DI contraction forces and HTI values first increased and then decreased. In addition, the size of the grain and primary particles gradually decreased with increasing pouring temperature. When the pouring temperature reached 740 °C, Li-containing oxide was distributed on the surface of the crack morphology and in the interior of the grains, easily leading to the initiation of cracks.

(2) With the mold temperature increasing from 200 to 400 °C, the length of spiral fluidity sample of the studied alloy increased from 293 to 736 mm, accompanied by a decrease in the DI contraction forces and HTI values. Once the mold temperature reached the critical value of 400 °C, some Li-rich oxides were distributed non-uniformly in the matrix, easily resulting in the initiation of cracks.

(3) To obtain good fluidity and hot-crack resistance of the Al−Li−Cu−Mg−Sc−Zr−Ti alloy simultaneously, the pouring temperature and mold temperature should be controlled below 740 and 400 °C, respectively. A pouring temperature of 720 °C and a mold temperature of 300 °C are more suitable for manufacturing the casting of the studied alloy.

CRediT authorship contribution statement

Yi-xiao WANG: Data curation, Formal analysis, Investigation, Validation, Visualization, Writing − Original draft, Review & editing; **Guo-hua WU:** Supervision, Funding acquisition; **Liang ZHANG:** Supervision, Writing − Review & editing; **You-jie GUO** and **Xin TONG:** Writing − Review & editing; **Liang-bin LI** and **Xun-man XIONG**: Investigation.

Declaration of competing interest

The authors declare that they have no known competing financial interests or personal relationships that could have appeared to influence the work reported in this paper.

Acknowledgments

References

[1] RIOJA J R, LIU J. The evolution of Al−Li base products for aerospace and space applications [J]. Metallurgical and Materials Transactions A, 2012, 43(9): 3325−3337.

[2] AHMED B, WU Su-Jun. Aluminum lithium alloys (Al−Li−Cu−X): New generation material for aerospace applications [J]. Applied Mechanics and Materials, 2013, 440: 104−111.

[3] WU Guo-hua, ZHANG Xiao-long, ZHANG Liang, WANG Yi-xiao, SHI Chun-chang, LI Pei-sen, REN Guang-xiao, DING Wen-jiang. An insight into the precipitate evolution and mechanical properties of a novel high-performance cast Al−Li−Cu−Mg−X alloy [J]. Journal of Alloys and Compounds, 2021, 875: 159996.

[4] XU Yuan-cai, LI Guang-yu, JIANG Wen-ming, ZHAN Jun-min, YU Yang, FAN Zi-tian. Investigation on characteristic and formation mechanism of porosity defects of Al−Li alloys prepared by sand casting [J]. Journal of Materials Research and Technology, 2022, 19: 4063−4075.

[5] QIN Ying, WU Guo-hua, ATRENS A, ZHANG Xiao-long, ZHANG Liang, DING Wen-jiang. Effect of NaOH concentration on microstructure and corrosion resistance of MAO coating on cast Al−Li alloy [J]. Transactions of Nonferrous Metals Society of China, 2021, 31(4): 913−924.

[6] RONG Mian, ZHANG Liang, WU Guo-hua, LI Wei-wei, ZHANG Xiao-long, SUN Jiang-wei, DING Wen-jiang. Effect of refining processes on inclusions and mechanical properties of cast Al−2Li−2Cu−0.2Zr alloy [J]. Transactions of Nonferrous Metals Society of China, 2019, 29(7): 1375−1382.

[7] RAVI K R, PILLAI R M, AMARANATHAN K R, PAI B C, CHAKRABORTY M. Fluidity of aluminum alloys and composites: A review [J]. Journal of Alloys and Compounds, 2008, 456(1/2): 201−210.

[8] TONG C H, YAO L G, NIEH C Y, CHANG C P, HSU S E. Castability of Al−Li−Mg and AL−Li−Cu−Mg alloys [J]. J Phys Colloques, 1987, 48(C3): 117−122.

[9] SAIKAWA S, SUGIOKA S, NAKAI K, SUGIURA Y, KAMIO A. Microstructure and mechanical properties of 8091 Al−Li alloys cast into permanent and sand molds [J]. Journal of Japan Institute of Light Metals, 1995, 45(5): 261−266.

[10] SAIKAWA S, NAKAI K, SUGIURA Y, KAMIO A. Effects of Zr and Ti contents on castability of Al−Li−Cu−Mg and Al−Li−Mg alloys [J]. Journal of Japan Foundry Engineering Society, 1997, 69(6): 469−476.

[11] LI Bing-cheng, ZHANG Jing, YE Fa-wang, TANG Ru-yue, DONG Quan, CHEN Jian-hao. An approach to studying the hot tearing mechanism of alloying elements in ternary Mg−Zn−Al alloys [J]. Journal of Materials Processing Technology, 2023, 317: 117980.

[12] LI Yue, LI Hong-xiang, KATGERMAN L, DU Qiang, ZHANG Ji-shan, ZHUANG Lin-zhong. Recent advances in hot tearing during casting of aluminium alloys [J]. Progress in Materials Science, 2021, 117: 100741.

[13] ESKIN D G, SUYITNO, KATGERMAN L. Mechanical properties in the semi-solid state and hot tearing of aluminium alloys [J]. Progress in Materials Science, 2004, 49(5): 629−711.

[14] YUAN Xue-liang, LIU Xin, ZUO Jian. The development of new energy vehicles for a sustainable future: A review [J]. Renewable and Sustainable Energy Reviews, 2015, 42: 298−305.

[15] WILLIAMS J C, STARKE JR E A. Progress in structural materials for aerospace systems [J]. Acta Materialia, 2003, 51(19): 5775−5799.

[16] KANG B K, SOHN I L. Effects of Cu and Si contents on the fluidity, hot tearing, and mechanical properties of Al−Cu−Si alloys [J]. Metallurgical and Materials Transactions A, 2018, 49(10): 5137−5145.

[17] WANG Yi-xiao, WU Guo-hua, ZHANG Liang, GUO You-jie, WANG Cun-long, LI Liang-bin, XIONG Xun-man. Enhanced strength and ductility in sand-cast Al−Li−Cu−Mg−Zr alloy via synergistic microalloying with Sc and Ti [J]. Journal of Alloys and Compounds, 2023, 962: 170954.

[18] ZHANG Jin-shuo, ZHONG Xiao-xiang, ZHANG Liang, WU Guo-hua, LIU Wen-cai. Effect of heat treatments on microstructure and mechanical properties of sand cast Al−2Li−2Cu−0.5Mg−0.2Sc−0.2Zr alloy [J]. Transactions of Nonferrous Metals Society of China, 2022, 32(2): 411−423.

[19] ZHANG Xiao-long, ZHANG Liang, WU Guo-hua, SUN Jiang-wei, RONG Mian, HSIEH C C, YU Yu-xiang. Influence of Sc content on the microstructure and mechanical properties of cast Al−2Li−2Cu−0.5Mg−0.2Zr alloy [J]. Materials Characterization, 2018, 142: 223−236.

[20] CAO G, HAYGOOD I, KOU S. Onset of hot tearing in ternary Mg−Al−Sr alloy castings [J]. Metallurgical and Materials Transactions A, 2010, 41(8): 2139−2150.

[21] CAO G, HAYGOOD I, KOU S. Hot tearing of ternary Mg−Al−Ca alloy castings [J]. Metallurgical and Materials Transactions A, 2006, 37(12): 3647−3663.

[22] ARGON A S, BIKERMAN J J. Physics of strength and plasticity [J]. Physics Today, 1971, 24(8): 60.

[23] GURSON A L. Continuum theory of ductile rupture by void nucleation and growth: Part I—Yield criteria and flow rules for porous ductile media [J]. Journal of Engineering Materials and Technology, 1977, 99(1): 2−15.

[24] GUO You-jie, ZHANG Liang, WU Guo-hua, WANG Yi-xiao, QI Fang-zhou, XU Xuan-xi, TONG Xin, LI Pei-sen, REN Guang-xiao, GENG Ying-jing, LI Liang-bin, XIONG Xun-man. Effect of Li content on hot-tearing susceptibility of ternary Al−Cu−Li alloys: Experimental investigation, criterion prediction, and simulation assessment [J]. Metallurgical and Materials Transactions A, 2023, 54(2): 4850−4867.

[25] GUO You-jie, ZHANG Liang, WU Guo-hua, WANG Yi-xiao, QI Fang-zhou, XU Xuan-xi, TONG Xin. Influence of Cu addition on hot tearing susceptibility and fluidity of Al−Li−Cu alloys: Experimental investigation, criterion prediction and simulation assessment [J]. Journal of Alloys and Compounds, 2023, 969: 172301.

[26] VINODH G, JAFARI NODOOSHAN H R, LI De-jiang, ZENG Xiao-qin, HU Bin, CARTER J T, SACHDEV A K. Effect of Al content on hot-tearing susceptibility of Mg−10Zn−xAl alloys [J]. Metallurgical and Materials Transactions A, 2020, 51(4): 1897−1910.

[27] HU Bo, LI Zi-xin, LI De-jiang, YING Tao, ZENG Xiao-qin, DING Wen-jiang. A hot tearing criterion based on solidification microstructure in cast alloys [J]. Journal of Materials Science & Technology, 2022, 105: 68−80.

[28] WANG Ke, FU Peng-huai, PENG Li-ming, WANG Ying-xin, DING Wen-jiang. A simplified hot-tearing criterion for shape castings based on temperature-field simulation [J]. Metallurgical and Materials Transactions A, 2019, 50(11): 5271−5280.

[29] ZHOU Ye, MAO Ping-li, WANG Zhi, ZHOU Le, WANG Feng, LIU Zheng. Experimental investigation and simulation assessment on fluidity and hot tearing of Mg−Zn−Cu system alloys [J]. Journal of Materials Processing Technology, 2021, 297: 117259.

[30] HU Bo, LI De-jiang, LI Zi-xin, WANG Xue-yang, ZENG Xiao-qin. Step-by-step observation of secondary-phase evolution during the casting cracking process in Mg−Ce−Al alloys [J]. Metallurgical and Materials Transactions A, 2022, 53(9): 3478−3492.

[31] HU Bo, LI De-jiang, YING Tao, YU Ning, ZENG Xiao-qin. Oxidation mechanism of molten Al−5Mg−2Si−Mn alloy [J]. Journal of Materials Science, 2020, 55(26): 12554−12567.

[32] AKHTAR N, AKHTAR W, WU S J. Melting and casting of lithium containing aluminium alloys [J]. International Journal of Cast Metals Research, 2015, 28(1): 1−8.

[33] DU Q, JACOT A. A two-dimensional microsegregation model for the description of microstructure formation during solidification in multicomponent alloys: Formulation and behaviour of the model [J]. Acta Materialia, 2005, 53(12): 3479−3493.

[34] STJOHN D H, PRASAD A, EASTON M A, QIAN M. The contribution of constitutional supercooling to nucleation and grain formation [J]. Metallurgical and Materials Transactions A, 2015, 46(11): 4868−4885.

[35] WANG Yi-xiao, WU Guo-hua, ZHANG Liang, GUO You-jie, WANG Cun-long, LI Liang-bin, XIONG Xun-man. Microstructure evolution and mechanical properties of a cast and heat-treated Al−Li−Cu−Mg alloy: Effect of cooling rate during casting [J]. Materials Science and Engineering: A, 2023, 880: 145366.

[36] SWEET L, EASTON M A, TAYLOR J A, GRANDFIELD J F, DAVIDSON C J, LU L M, COUPER M J, STJOHN D H. Hot tear susceptibility of Al−Mg−Si−Fe alloys with varying iron contents [J]. Metallurgical and Materials Transactions A, 2013, 44(12): 5396−5407.

浇注温度和模具温度对铸造 Al–Li–Cu–Mg–Sc–Zr–Ti 合金流动性和热裂行为的影响

王一笑 [1]，吴国华 [1]，张 亮 [1]，郭幼节 [1]，童 鑫 [1]，李良彬 [2]，熊训满 [2]

1. 上海交通大学 材料科学与工程学院 轻合金精密成型国家工程研究中心和金属基复合材料国家重点实验室，上海 200240；

2. 江西赣锋锂业有限公司，新余 338004

摘　要：通过实验与模拟方法研究了浇注温度和模具温度对 Al–2Li–2Cu–0.5Mg–0.15Sc–0.1Zr–0.1Ti 合金流动性和热裂行为的影响。结果表明，当浇注温度从 680 ℃升高到 740 ℃时，螺旋流动性试样的长度从 302 mm 增加到 756 mm；当模具温度从 200 ℃升到 400 ℃时，螺旋流动性试样的长度从 293 mm 增加到 736 mm。随着浇注温度和模具温度的升高，合金热裂敏感因子先降低后升高，主要是由于浇注温度过高容易产生含锂氧化物。过高的浇注温度和模具温度容易产生氧化物夹杂物和孔洞，导致合金的流动性降低，热裂敏感因子升高，综合实验和模拟结果分析可知，浇注温度和模具温度分别控制在~720 ℃和~300 ℃适合生产铸造铝锂合金产品。

关键词：浇注温度；模具温度；流动性；热裂行为；铸造铝锂合金；数值模拟

(Edited by Wei-ping CHEN)